Chemosphere 261 (2020) 128157

Contents lists available at ScienceDirect

Chemosphere

journal homepage: www.elsevier.com/locate/chemosphere

Fabrication and characterization of porous titanium-based PbO_2 electrode through the pulse electrodeposition method: Deposition condition optimization by orthogonal experiment☆

Guo Hua [a], Xu Zhicheng [a], Qiao Dan [a], Wan Dan [b], Xu Hao [a, *], Yan Wei [a], Jin Xiaoliang [b]

[a] Department of Environmental Science and Engineering, Xi'an Jiaotong University, Xi'an, 710049, PR China
[b] Shaanxi Zhengwei Environmental Testing CO,. LTD, Xi'an, 710049, PR China

HIGHLIGHTS

- Novel PbO_2 anodes were fabricated through pulse electrodeposition.
- The effects of pulse electrodeposition parameters on PbO_2 characters were evaluated.
- An optimized pulsed electrodeposition parameter is presented.
- The brief mechanism of pulse electrodeposition is uncovered.

ARTICLE INFO

Article history:
Received 5 June 2020
Received in revised form
21 August 2020
Accepted 25 August 2020
Available online 28 August 2020

Handling Editor: Dr. E. Brillas

Keywords:
PbO_2 electrode
Pulse electrodeposition
Deposition condition
Orthogonal optimization
Porous titanium

ABSTRACT

Porous titanium-based PbO_2 electrodes were successfully fabricated by pulse electrodeposition method. The primary pulse electrodeposition parameters, including pulse frequency (f), duty ratio (γ), average current density (J_a) and electrodeposition time (t) were considered in this study. An orthogonal experiment was designed based on those four factors and in three levels. SEM images and XRD results suggest that the surface morphology and structure of PbO_2 electrodes could be easily changed by varying pulse electrodeposition parameters. Orthogonal analysis reveals that the increase of f and J_a could decrease the average grain size of PbO_2 electrodes, which is conducive to create more active sites and promote the generation of hydroxide radicals. The electrochemical degradation of Azophloxine was carried out to evaluate the electrochemical oxidation performance of pulse electrodeposited electrodes. The results indicate that the influences of four factors can be ranked as follow: $J_a > \gamma \approx t > f$. The higher f, larger J_a and longer t could facilitate the optimization of the integrated electrochemical degradation performance of prepared PbO_2 electrode. The accelerated life time is dominated by J_a and t, coincident with the average weight increase of β-PbO_2 layer. The optimal parameters of pulse electrodeposition turn out to be: $f = 50$ Hz, $\gamma = 30\%$, $J_a = 25$ mA cm^{-2}, $t = 60$ min. Together, the consequences of the experiments give assistance to uncover and roughly conclude the mechanism of pulse electrodeposition.

1. Introduction

Electrochemical advanced oxidation is an attractive and promising technique for organic pollutants removal because of its environmental friendliness, easy accessibility and mineralization effectiveness (Nidheesh et al., 2018; Zhang et al., 2019a). In electrochemical advanced oxidation process, strong oxidizing agents are generated in the vicinity of anode to degrade the organics into carbon dioxide, water and inorganic ions (Miklos et al., 2018; Yang et al., 2019; Yao et al., 2019a).

Anode material plays a crucial role during electrochemical oxidation process, directly influencing the efficiency of the degradation and mineralization for targeted contaminants (Xu et al., 2019c; Yao et al., 2019b; Zahorulko et al., 2019). Therefore, a series of anode materials have been investigated in previous works,

☆ All conflict of interest disclosures: None.

* Corresponding author.
E-mail addresses: shohoku777@stu.xjtu.edu.cn (G. Hua), Kylezcxu@foxmail.com (X. Zhicheng), 18091276816@163.com (Q. Dan), 184295439@qq.com (W. Dan), xuhao@mail.xjtu.edu.cn (X. Hao), yanwei@xjtu.edu.cn (Y. Wei), 1364687589@qq.com (J. Xiaoliang).

https://doi.org/10.1016/j.chemosphere.2020.128157
0045-6535/

such as SnO_2 (Bi et al., 2019; Chen et al., 2019; Zhang et al., 2019c), boron-doped diamond (BDD) (Mei et al., 2019; Cornejo et al., 2020; Suzuki et al., 2020), IrO_2 (Hu et al., 2014; Baddouh et al., 2019; Sun et al., 2020), PbO_2 (Wang et al., 2019; Zhou et al., 2020), Ti_4O_7 electrode (Lin et al., 2018; Wang et al., 2020), and compound electrodes (Yuan et al., 2019; Shao et al., 2020). Pure SnO_2 is an n-type semiconductor with low conductivity at room temperature, which needs to be improved by various elements doping (Rao and Venkatarangaiah, 2014). BDD electrode shows an extremely wide potential window, but is restricted in the large-scale application due to its high cost of synthesis, while IrO_2 electrode is favorable to oxygen evolution side reaction because of its low oxygen evolution potential (OEP) (Panizza and Cerisola, 2009). Ti_4O_7, a Magnéli phase titanium sub-oxide, is proposed as a promising anode material for its great conductivity and chemical stability, however the passivation during anodic polarization is still a problem to be further addressed (Chaplin, 2014).

Among them, PbO_2 electrode has been widely applied in electrochemical oxidation because of its prominent electro-catalytic performance, mineralization effect and low cost (Dargahi et al., 2019; Qian et al., 2019; Tammam and Hassan, 2019). However, there are still some drawbacks of PbO_2 electrode requiring improvement, such as Pb leakage, low hydroxide radical utilization and OEP. In order to solve those problems, many efforts have been made by different approaches, including substrate and inner layer modification (SnO_2–Sb inner layer (Yu et al., 2018; Xu et al., 2019b), TiO_2 nanotubes inner layer (Wang et al., 2018; Wu et al., 2019), carbon nanotubes inner layer (Xu et al., 2019a), stainless steel substrate (Elaissaoui et al., 2019)), elements doping (Xia and Dai, 2018; Bian et al., 2019; Chen et al., 2020), particle incorporation (Duan et al., 2019; Tang et al., 2020) and surfactant modification (Duan et al., 2018; Velichenko et al., 2020).

Moreover, the change of PbO_2 fabrication technique also could lead significant variation of electrode morphology and property (Boukhchina et al., 2019). Recently, pulse electrodeposition method was introduced to PbO_2 electrodes preparation in order to increase surface active site and improve the electrocatalytic capability of PbO_2 electrode (Hakimi et al., 2019). He et al. (2018) investigated the effect of different duty cycles in pulse reverse current (PRC) electrodeposition, and pointed out that crystal structure and morphology of PbO_2 observably altered after PRC deposition, which rise the content of β phase and create a rough surface of morphologic feature. Yao et al. (2017) explored the effects of peak current density on the characteristics of PbO_2–CeO_2 nanocomposite electrodes, of which the results showed that the increase of peak current density could make the morphology finer and more compact, as well as reduce the crystal size. Various parameters of pulse electrodeposition have been severally investigated in detail, whereas, the parameters are not complete independent with each other. The relations among those factors show as follows:

$$f = \frac{1}{T_p + T_v} \tag{1}$$

$$\gamma = \frac{T_p}{T_p + T_v} \tag{2}$$

$$J_a = \left(J_p + J_v\right)\gamma \tag{3}$$

where f is the frequency, T_p is the peak value time, T_v is the valley value time, γ is the duty ratio, J_a is the average current density, J_p is the peak value current density and J_v is the valley value current density. Therefore, it is necessary to study the comprehensive effects of different pulse electrodeposition parameters on the characteristics of PbO_2 electrode.

In this study, porous titanium based PbO_2 electrodes were fabricated through pulse electrodeposition method. Porous titanium, a common anti-corrosion filter element, was chosen as the substrate material of PbO_2 electrode, because the porous structure could improve the specific surface area of electrodes. Orthogonal experiment was designed to explore the optimum pulse electrodeposition parameters and systematically analyze the influences of each parameter on the electrode properties. The most important operating parameters of pulse electrodeposition, including pulse frequency (f), duty ratio (γ), average current density (J_a) and the time (t) of electrodeposition, were selected as four factors, along with three levels under every factor. L9 orthogonal array were chosen for this work. The normal PbO_2 electrode fabricated by direct current electrodeposition was assigned as the control group. The prepared PbO_2 electrodes were characterized by scanning electron microscopy (SEM), X-ray diffraction (XRD), cyclic voltammetry (CV) sweep and electrochemical impedance spectroscopy (EIS). The hydroxide radical productivities of prepared electrodes were also tested in order to estimate the electrochemical oxidation capabilities. Following from that, the prepared electrodes were used as the anodes for the electrochemical degradation of Azophloxine (AR1) for purpose of the comprehensive electrochemical degradation performance evaluation. Ultimately, the electrode stabilities were characterized by the accelerated lifetime and the elements leakage tests. Furthermore, the pulse electrodeposition mechanisms are briefly summarized based on the results.

2. Materials and methods

2.1. Materials

All chemicals used in this work purchased from Sinopharm Chemical Reagent Co., Ltd, were of analytical grade without further purification. The aqueous solutions were deionized water (18 MΩ cm^{-1}, EPED-S2-D, Nanjing, China). Unless otherwise specified, all the experiments were done at room temperature.

2.2. Preparation of substrates and fabrication of inner layer

Porous titanium plates (Filter Fineness = 80 μm, Baoji Yinggao metal material Ltd., China) with a dimension of 2 cm × 5 cm × 1 mm were used as the electrode substrate. The pretreatment of porous Ti plate and introduction of intermediate Sb–SnO_2 layer and α-PbO_2 layer were the same as our previous work (Li et al., 2016a, 2016b, 2017; Wu et al., 2019).

2.3. Electrodeposition of surface β-PbO_2 layer

The surface β-PbO_2 layer was coated on the Ti/Sb–SnO_2/α-PbO_2 electrode via anodic deposition process. The plating bath was composed of 0.5 M $Pb(NO_3)_2$, 0.2 M $Cu(NO_3)_2$ and 0.01 M NaF. The solution pH value was adjusted to 2.0 with the concentrated HNO_3.

2.3.1. Direct current electrodeposition

Setting the current density as 20 mA cm^{-2}, the temperature was controlled at 65 °C for 120 min for the direct current deposition processing. The same titanium mesh served as the counter cathode. And we marked the fabricated electrodes as PbO_2(DC).

2.3.2. Design of orthogonal experiment

The pulse electrodeposition processes were conducted at 65 °C, the valley value current density was maintained at 0 mA cm^{-2}, so the peak value current density could be determined by the γ and the J_a. The titanium mesh with the same dimension served as the

counter cathode.

The primary electroplating parameters of f, γ, J_a and t were considered in this study. This experiment was designated as $L_9(3^4)$ orthogonal array, which chose four plating parameters and three levels. The factors and levels of the orthogonal experiment are listed in Table SM-1, and the L9 orthogonal arrays are presented in Table SM-2.

As shown in Fig. 1, the fabricated electrodes were marked as PbO_2(P1~9) respectively, in accordance with the experiment number in Table SM-2. Furthermore, all test results from pulse electrodeposition electrodes (PbO_2(P1~9)) in this work would be normalized with that from constant current electrodeposition (PbO_2(DC)) as the base, before doing orthogonal analysis. The data were normalized as follow:

$$X_i' = \frac{X_i}{X_{DC}} \tag{4}$$

where X_i' is the normalization coefficient of X_i, X_i is the test result of $PbO_2(P_i)$, i is the experiment number in Table SM-2, X_{DC} is the test result of PbO_2(DC).

2.4. Characterization

SEM (Techcomp, SU3500) was employed for characterizing the surface morphology of samples. XRD (SHIMADZU, XRD-6100) analyses were performed using a diffractometer with Cu-Kα radiation.

A three-electrode cell was adopted to perform all electrochemical measurements at room temperature. The prepared electrodes act as the working electrodes, respectively. Ag/AgCl/saturated KCl electrode was selected as the reference electrode and platinum sheet as counter electrode. CV sweep was conducted in 0.5 M Na_2SO_4 solution at 10 mV s^{-1} in the range of 0–2.5 V. EIS measurement was conducted in 0.5 M Na_2SO_4 solution with a measurement potential of 0 V (vs Ag/AgCl), of which the frequencies swept from 10^5 Hz to 10^{-2} Hz with a sine wave in 5 mV amplitude.

The electrochemical oxidation capacity was assessed by comparison for the yields of hydroxyl radical (·OH) from different electrodes. The HPLC (Sykam, S500) with dimethyl sulfoxide (DMSO) trapping was used to test the ·OH concentration after 1-h electrolysis (Xu et al., 2018).

The accelerated lifetime tests were conducted at constant current density of 500 mA cm^{-2} in 3 M H_2SO_4 for electrode stability evaluation (35 °C ± 2 °C). The titanium mesh act as the counter electrode. The prepared electrode was employed as the working electrode, which was deemed as deactivation when the cell voltage came to 10 V.

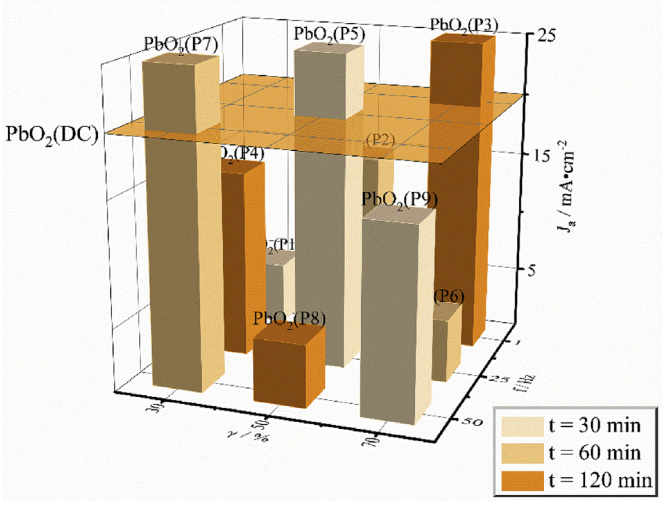

Fig. 1. Orthogonal experimant design of pulse electrodeposition.

2.5. Electrochemical oxidation test

The electrochemical oxidation for Azophloxine (AR1, $C_{18}H_{13}N_3NaO_8S_2$, CAS no. 3734-67-6) were implemented in 250 mL synthesized wastewater containing 200 mg L^{-1} AR1 with 10 g L^{-1} Na_2SO_4 as the supportive electrolyte. The electrode prepared was used as the anode and titanium mesh as the cathode. The distance between anode and cathode was maintained at 1.0 cm. The electrochemical oxidation process was carried out in constant current of 30 mA cm^{-2} (the working electrode area of 10 cm^2) with a magnetic stirrer for 120 min. The samples were monitored and analyzed every 30 min. UV–Vis absorption (UV2600A, Unico, Shanghai, China) was employed to test the concentration of AR1 at the characteristic wavelength of 506 nm (Zhang et al., 2019b; Lei et al., 2020). COD was measured by a commercial COD detector (Multi Direct, Lovibond), and TOC was assayed by ET1020A TOC analyzer.

The % of COD removal (R_{COD}) and % of TOC removal (R_{TOC}) of AR1 in electrochemical degradations were calculated as follows:

$$R_{COD} = \frac{COD_0 - COD_t}{COD_0} \times 100\% \tag{5}$$

$$R_{TOC} = \frac{TOC_0 - TOC_t}{TOC_0} \times 100\% \tag{6}$$

where COD_0 and COD_t are the chemical oxygen demands, TOC_0 and TOC_t are the total organic carbon at the initial and end, respectively.

In addition, the electrochemical oxidation effect of the PbO_2 electrodes on AR1 was assessed through average current efficiency (ACE) and energy consumption per unit COD mass (EC_{COD}, kWh $gCOD^{-1}$), which were calculated as follows:

$$ACE = \frac{COD_0 - COD_t}{8It} FV \times 100\% \tag{7}$$

$$EC_{COD} = \frac{UIt}{(COD_0 - COD_t)V} \tag{8}$$

where F is the Faraday constant (96,487 C mol^{-1}), V is the volume of the electrolyte (L), I is the current (A), t is the time (min) and U is the cell voltage (V).

Additionally, degradation index (DI) was established in order to compare the electrochemical oxidation performance of pulse electrodeposition electrodes. The DI was calculated as follow:

$$DI = R_{COD}' + R_{TOC}' + GCE' - EC_{COD}' \tag{9}$$

where R_{COD}', R_{TOC}', ACE' and EC_{COD}' are the normalization coefficients of R_{COD}, R_{TOC}, ACE and EC_{COD}, respectively.

3. Results and discussion

3.1. Surface morphology and structure

As shown in Fig. 2, the surface morphology of prepared electrodes indicates significant differences of structure and particle size among those. Following the raising of t and J_a, a significant increase in PbO_2 particle size was recorded. In Fig. 2c, d, 2e, 2f and 2h, there

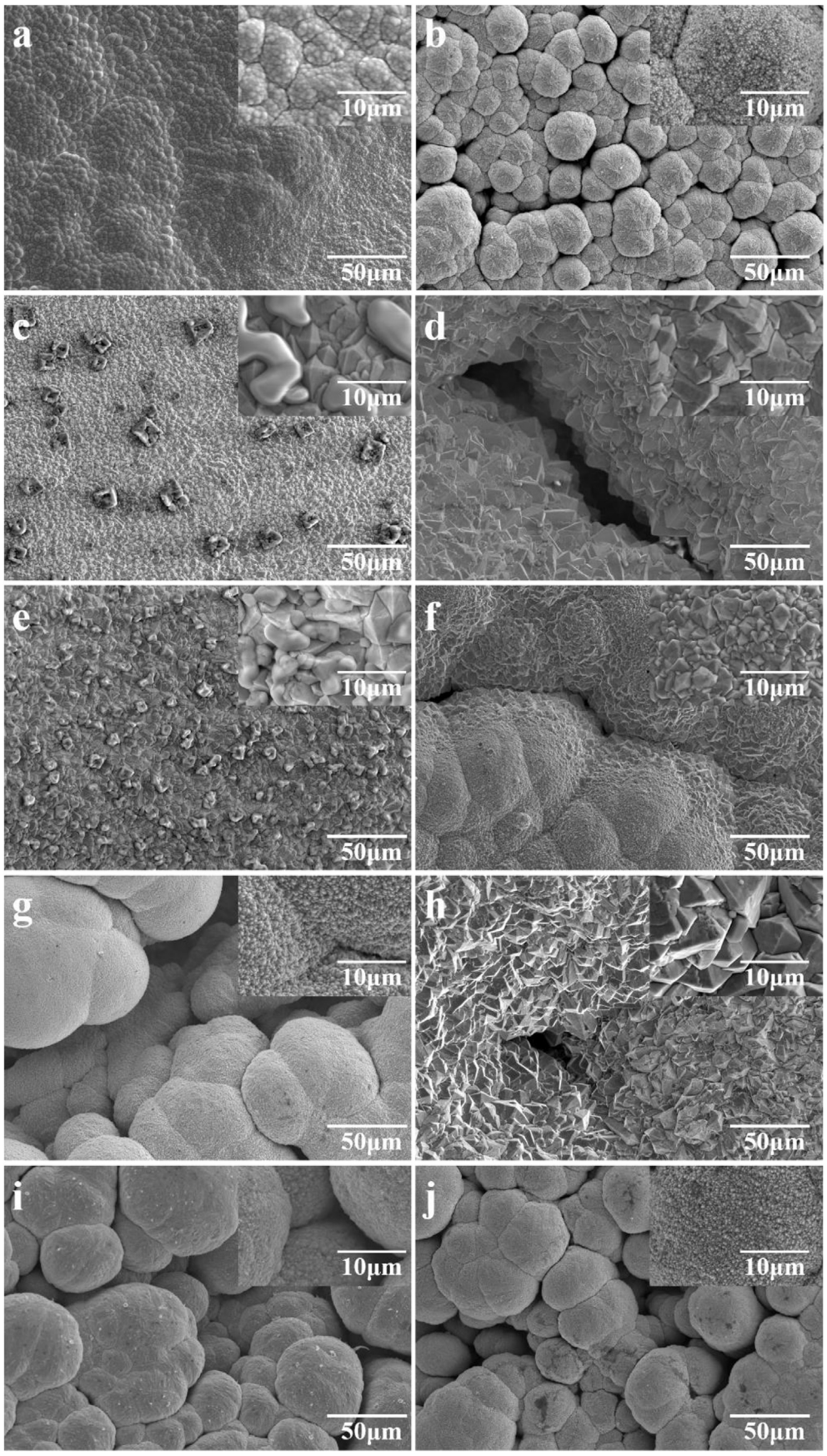

Fig. 2. SEM images of prepared electrodes, (a) PbO_2(DC), (b) PbO_2(P1), (c) PbO_2(P2), (d) PbO_2(P3), (e) PbO_2(P4), (f) PbO_2(P5), (g) PbO_2(P6), (h) PbO_2(P7), (i) PbO_2(P8), (j) PbO_2(P9).

are typical pyramidal shape, while some indefinite shape could be observed in Fig. 2c, e and 2f, coincident with findings in other reports (Elaissaoui et al., 2019; Ansari and Nematollahi, 2020). Interestingly, three-dimensional cauliflower shape which could be fabricated by Ce doping (Lyu et al., 2019), was frequently observed in the electrodes made by pulse electrodeposition with high f and γ. The PbO_2 electrodes deposited in methanesulfonate bath showed the same fine and compact surface morphology without three-dimensional structure (He et al., 2019). As shown in Fig. SM-1, porous titanium was chosen as the substrate of PbO_2 electrodes to expand the surface area. The surface morphology and porous structure were improved by acid etch and inner layer coating. It is apparent from Fig. 2 that surface PbO_2 layer shows porous morphology in every prepared electrode except PbO_2(DC), PbO_2(P2) and PbO_2(P4), which means that porous PbO_2 layer could be formed more easily under high frequency pulse. Moreover, the uniform and compact surface could be obtained on the electrodes deposited in high frequency pulse, which may be because the pulse electrodeposition has ability to alleviate the concentration polarization during the fabrication process (shown as Fig. 4).

Fig. 3 displays XRD patterns of the prepared electrodes by the constant current electrodeposition and the pulse electrodeposition. What stands out in Fig. 3 is the presences of α-PbO_2 in pulse deposition PbO_2 electrodes, compared with PbO_2(DC). The diffraction peaks located at 25.39°, 31.94°, 36.16° and 49.13° correspond to the lattice planes (110), (101), (200) and (211) of β-PbO_2 (75-2420)

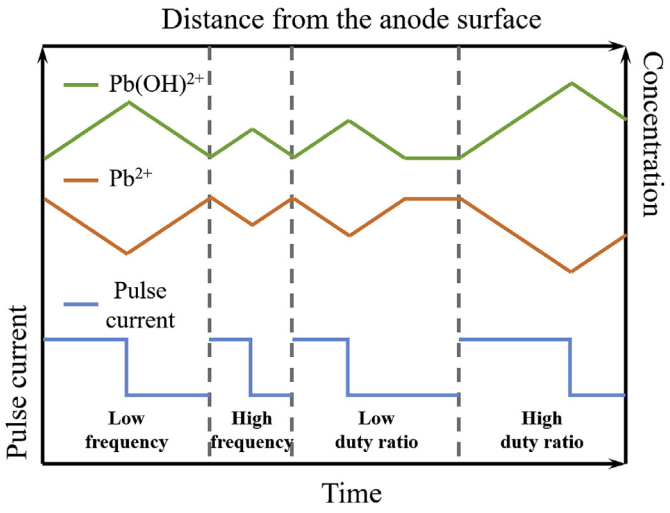

Fig. 4. Concentration variations of Pb^{2+} and $Pb(OH)^{2+}$ in the electrolyte during pulse electrodeposition processes with different parameters.

respectively. The other characteristic peaks at 28.40°, 32.63°, 36.02°, 38.40°,39.81°,44.92°, 49.32° and 52.35° correspond to the lattice planes (111), (002), (200), (121), (112), (022), (202) and (131) of α-PbO_2 (75-2414) respectively. It may prove that pulse

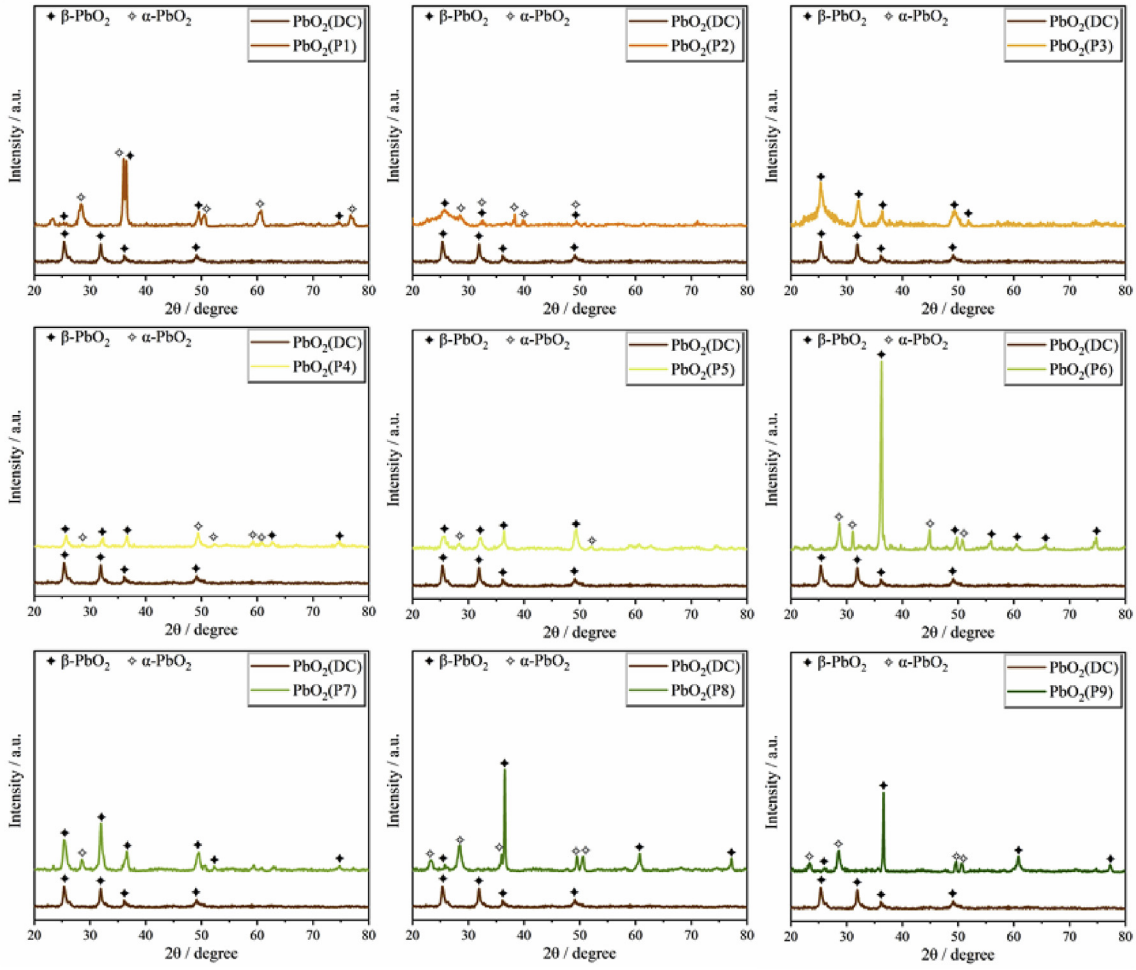

Fig. 3. XRD patterns of prepared electrodes.

electrodeposition can change the crystallization process of PbO_2. Comparing the XRD patterns in Fig. 3, the electrodes (PbO_2(3), PbO_2(5), PbO_2(7)) belonging to high J_a (J_a = 25 mA cm^{-2}) group mainly show diffraction peaks of β-PbO_2, which may indicate that high J_a is beneficial to form pure β-PbO_2. Moreover, it is clear that the diffraction patterns of PbO_2(P7), PbO_2(P8) and PbO_2(P9) are sharp and strong, demonstrating that well-crystallized PbO_2 could be obtained by pulse electrodeposition with high frequency.

The average grain sizes of surface PbO_2 crystal are presented in Table 1, which were calculated by Debye−Scherrer equation:

$$D = \frac{k\lambda}{\beta \cos\theta} \tag{10}$$

where D is the crystallite size, λ is the X-ray wavelength, β is the full width at half maximum of the strongest diffraction peak and θ is the diffraction angle. After normalization and orthogonal analysis of grain size data (shown in Table SM-3), it could be concluded that J_a and f are the primary influence factors on grain size. The PbO_2 nucleation mechanism can be illustrated as Eq. 11–13 (Sun et al., 2019). When current is applied at the anode, a small quantity of adsorbed ·OH are initially generated on the anode surface (Eq. (11)). The aqueous Pb^{2+} would diffuse toward the anode surface via convective diffusion and then react with ·OH with the formation of the soluble intermediates ($Pb(OH)^{2+}$) by Eq. (12), eventually, the $Pb(OH)^{2+}$ is electrochemically oxidized to PbO_2 (Eq. (13)).

$$H_2O \rightarrow \cdot OH_{ads} + H^+ + e^- \tag{11}$$

$$Pb^{2+} + \cdot OH_{ads} \rightarrow Pb(OH)^{2+} \tag{12}$$

$$Pb(OH)^{2+} + H_2O \rightarrow PbO_2 + 3H^+ + e^- \tag{13}$$

There was a significant negative correlation between J_a and average grain size. In other word, increase of J_a is helpful to minify PbO_2 crystal, coincident with traditional PbO_2 electrodeposition mechanism (Velichenko et al., 2009; Sirés et al., 2010). Nonetheless, the analysis result revealed that PbO_2 average grain size increased sharply when f reached 50 Hz, attributed to the poly-crystal aggregate occurring in high frequency pulse.

Combine previous studies about cathodic pulse electrodeposition mechanism (Ye et al., 2018, 2020), Fig. 4 illustrates the concentration variations of Pb^{2+} and $Pb(OH)^{2+}$ in the electrolyte during pulse electrodeposition processes with different parameters. Crystal size is determined together by nucleation and growth process. On the one hand, high J_a brings more nucleation, which helps to form small crystal. On the other, high f diminishes concentration polarization effectively, which could promote high valence state metal ion migration then restrain nucleation process, therefore growth process rules in electrodeposition and crystal size increases. The increase of γ could however impair the influence resulted from high f, driving the process to present more similarly to direct electrodeposition. Interestingly, the average grain size of PbO_2(P7) was smaller than that of other electrodes made by high frequency pulse. It means that when J_a reached 25 mA cm^{-2}, nucleation was strong enough to re-dominate the electrodeposition process, resulting in the small size of PbO_2 crystal. To sum up, there is no change of electrodeposition mechanism in essence after introducing pulse current supply mode, whereas it is notably that, through regulating the pulse parameters, the crystal nucleation and growth process could be balanced so as to optimize the structure ad morphology of fabricated PbO_2 electrode.

3.2. Electrochemical test

3.2.1. CV

Fig. SM-2 shows the CV curves of prepared PbO_2 electrodes. The anodic peaks appeared on approximately 1.25 V, because PbO_2 is a nonstoichiometric compound and the ratio of oxygen to lead was lower than the stoichiometric ratio, so that some low-valent lead compounds in the active layer were oxidized to that of high-valent. The upsurge of anodic current can be observed at 1.8–2.0 V for all electrodes, which could be attributed to oxygen evolution reaction. It could be seen that the current responses are enhanced prominently by pulse electrodeposition, which indicates that pulse electrodeposition favors charge exchange. PbO_2(P7) shows the highest current response, which means the superior conductivity of PbO_2(P7). Table 1 presents the OEP and voltammetric charge which were calculated from CV test. The highest (1.94 V) and lowest (1.84 V) OEP were obtained at PbO_2(P5) and PbO_2(DC) respectively, similar to other porous PbO_2 electrode (Liu et al., 2017). It therefore could be interpreted that partial α-PbO_2 presence would not make distinct difference to the OEP of PbO_2 electrode. The electrochemical activity of an electrode can be evaluated through the voltammetric charge (q^*), related to the number of active sites. Higher value of q^* represents greater electrode activity for the identical electrode material. The q^* was acquired via integrating the cycle voltammetric curves over the entire potential range from 0 to 2.5 V (Xu et al., 2016). The results of calculation and orthogonal analysis of voltammetric charge (Fig. 5a and Table SM-4) shows that f was the dominating influence factor which positively correlated to voltammetric charge significantly. It could be explained by the results of SEM and XRD that high frequency pulse avails to form well crystallized, finer and porous surface PbO_2 layer, which is favorable to build more active sites and promote electrochemical oxidation ability (Wang et al., 2017; Weng and Yu, 2019).

3.2.2. EIS

EIS test results and equivalent circuit are shown in Fig. 5b and Table SM-5. The equivalent circuit and the simulation of parameters of EIS spectra were evaluated by ZSimDemo software, which indicated that the test data of all prepared electrodes well fitted in the

Table 1
Various characterization parameters of prepared electrodes.

Sample	Crystal size (nm)	OEP (V)	Voltammetric charge (C cm^{-2})	Accelerated lifetime (h)
PbO_2(DC)	17.7	1.84	1.33	152
PbO_2(P1)	30.1	1.90	1.58	138
PbO_2(P2)	13.6	1.92	0.87	192
PbO_2(P3)	14.4	1.94	0.84	268
PbO_2(P4)	15.3	1.91	0.7	272
PbO_2(P5)	9.5	1.94	1.44	173
PbO_2(P6)	27.1	1.89	1.58	137
PbO_2(P7)	16.9	1.93	1.48	212
PbO_2(P8)	41.2	1.89	1.8	158
PbO_2(P9)	40.2	1.88	1.87	146

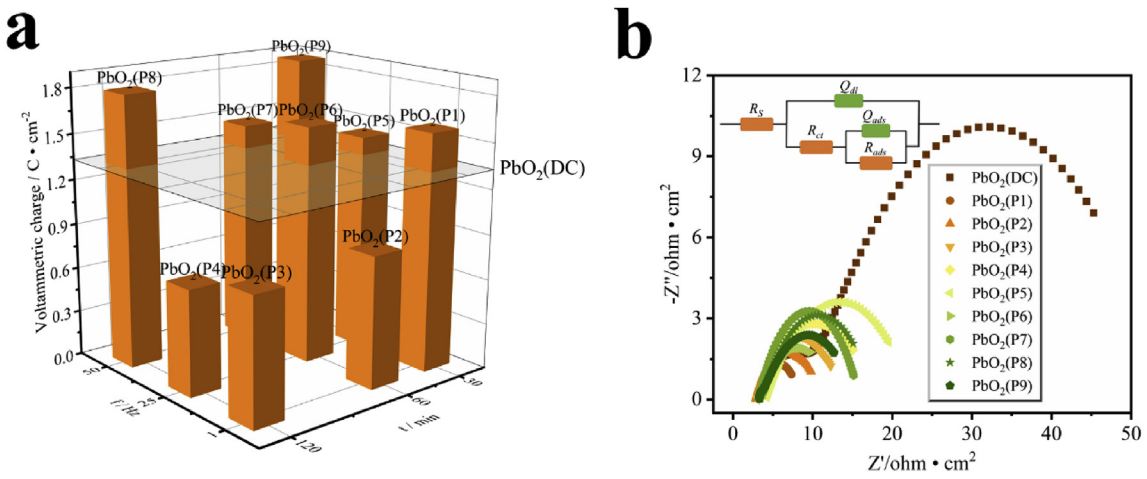

Fig. 5. (a) Voltammetric charge of prepared PbO_2 electrodes, (b) Nyquist diagrams and equivalent circuit of prepared PbO_2 electrodes.

equivalent circuit in Fig. 6. R_s represents the uncompensated solution resistance; CPE_1 the double layer capacitance (Q_{dl}); R_{ct} the charge transfer resistance; CPE_2 the adsorption pseudo capacitance of the reaction intermediates (Q_{ads}); R_{ads} the resistance imposed by the reaction intermediates adsorbed at the electrode surface (Yang et al., 2012). As can be seen from the figure above, the arc diameters of electrodes fabricated by pulse electrodeposition is significantly smaller than that of PbO_2(DC), which further supports the conclusion from CV that pulse electrodeposition is conducive to charge exchange.

3.3. Productivity of hydroxide radical

OH are generated from the oxidation of water, as shown in Eq. (14), which is the core of electrocatalytic reaction (Lei et al., 2020; Yijing Xia, 2020):

$$H_2O \rightarrow \cdot OH + H^+ + e^- \quad (14)$$

·OH were measured by an indirect method with dimethyl sulfoxide (DMSO) as the capture agent. ·OH reacts with DMSO to generate formaldehyde, then with 2, 4-dinitrophenylhydrazine (DNPH) to generate corresponding hydrazone (HCHO-DNPH), and is finally detected by HPLC. The content of ·OH can be calculated by the content of formaldehyde, which could be determined by HPLC. Fig. SM-3 compares the ·OH productivities of pulse electrodeposition PbO_2 electrodes and PbO_2(DC). The ·OH concentrations of the electrodes fabricated by pulse electrodeposition were all higher than that of PbO_2(DC). Combining with the results of XRD, a possible explanation is that the decrease of crystal size and porous morphology could create more active sites to accelerate ·OH production.

The result of normalization and orthogonal analysis (listed as Table SM-6) reveals the positive correlation between hydroxide radical productivity and t. And γ, which directly affects real deposition time, also facilitate hydroxide productivity. Those two correlations suggest that the real electrodeposition time should not be too short otherwise hydroxide radical productivity will be impaired. However, the primary factor that affects hydroxide radical productivity is f. In addition, the productivity of ·OH would be raised prominently by high frequency pulse, which is coincident with the orthogonal analysis result of voltammetric charge.

3.4. Electrochemical oxidation performance

Fig. 6 and Fig. SM-4 display the results of AR1 degradation in order to identify the electrode with the best electrochemical oxidation performance. Fig. SM-4 shows that simulated AR1 wastewater were decolorized after 120-min electrochemical oxidation. R_{COD} data of pulse electrodeposition electrodes were compared with that of PbO_2(DC) in Fig. 6a. As shown in Fig. 6b, the $ln(C_t/C_0)$ of COD test results were well fitted in pseudo-first-order kinetic. Except PbO_2(P1) and PbO_2(P6), R_{COD} of all electrodes fabricated by pulse electrodeposition were higher than that of PbO_2(DC). The electrodes belonging to high frequency group ($f = 50$ Hz) presented better COD removal capacity than others. In addition, PbO_2(P7) attained the highest R_{COD} (82.3%) which was 1.4 times higher than PbO_2(DC), as well as the highest k value which is 1.6 times as high as PbO_2(DC). R_{TOC} is an important index to evaluate the mineralization capacity of electrodes. From Fig. 6e and Table SM-7, it could be seen that PbO_2(P3), PbO_2(P5) and PbO_2(P7) electrodeposited in high J_a pulse performed better mineralization effect. According to XRD results, a possible explanation is that β-PbO_2 proportion, which can be increased by raising J_a during pulse electrodeposition, is important to enhance the mineralization ability of PbO_2 electrode. For the consideration of energy conservation, ACE and EC_{COD} are necessary to assess the electrochemical oxidation performance of electrode materials. Fig. 6c and d compare ACE and EC_{COD} between prepared electrodes respectively, and the data of those could be found in Table SM-7. PbO_2(P2) showed the highest ACE (12% improvement over PbO_2(DC)) and the lowest EC_{COD} (24% reduction under PbO_2(DC)), but the R_{COD} and R_{TOC} of PbO_2(P2) were insufficient than satisfactory target. Hence, DI (the computing method was showed in Eq. (9)) was introduced to evaluate and compare the electrochemical oxidation performance of prepared electrodes comprehensively and expediently. Fig. 6f exhibits the comparison of DI, where most pulse electrodeposition electrodes performed greater electrochemical degradation capacity of AR1. Meanwhile, PbO_2(P7) showed the best degradation capacity, which was 41% higher than PbO_2(DC) in degradation, and further exhibited the more favorable performance than PbO_2(DC) in all aspects.

The orthogonal analysis results of DI (shown as Table SM-8) suggest that the influences of four factors can be ranked as follow: $J_a > \gamma \approx t > f$. The large J_a, long t, moderate γ and high f are conducive to optimize the whole electrochemical degradation performance of PbO_2 electrode. Large J_a and long t are helpful to promote β-PbO_2 layer attachment. Besides, the coordination of moderate γ and high f is in favor of properly porous and compact surface structure. All of them improve the COD and TOC removal ability of PbO_2 electrode together, and the current efficiency is also optimized.

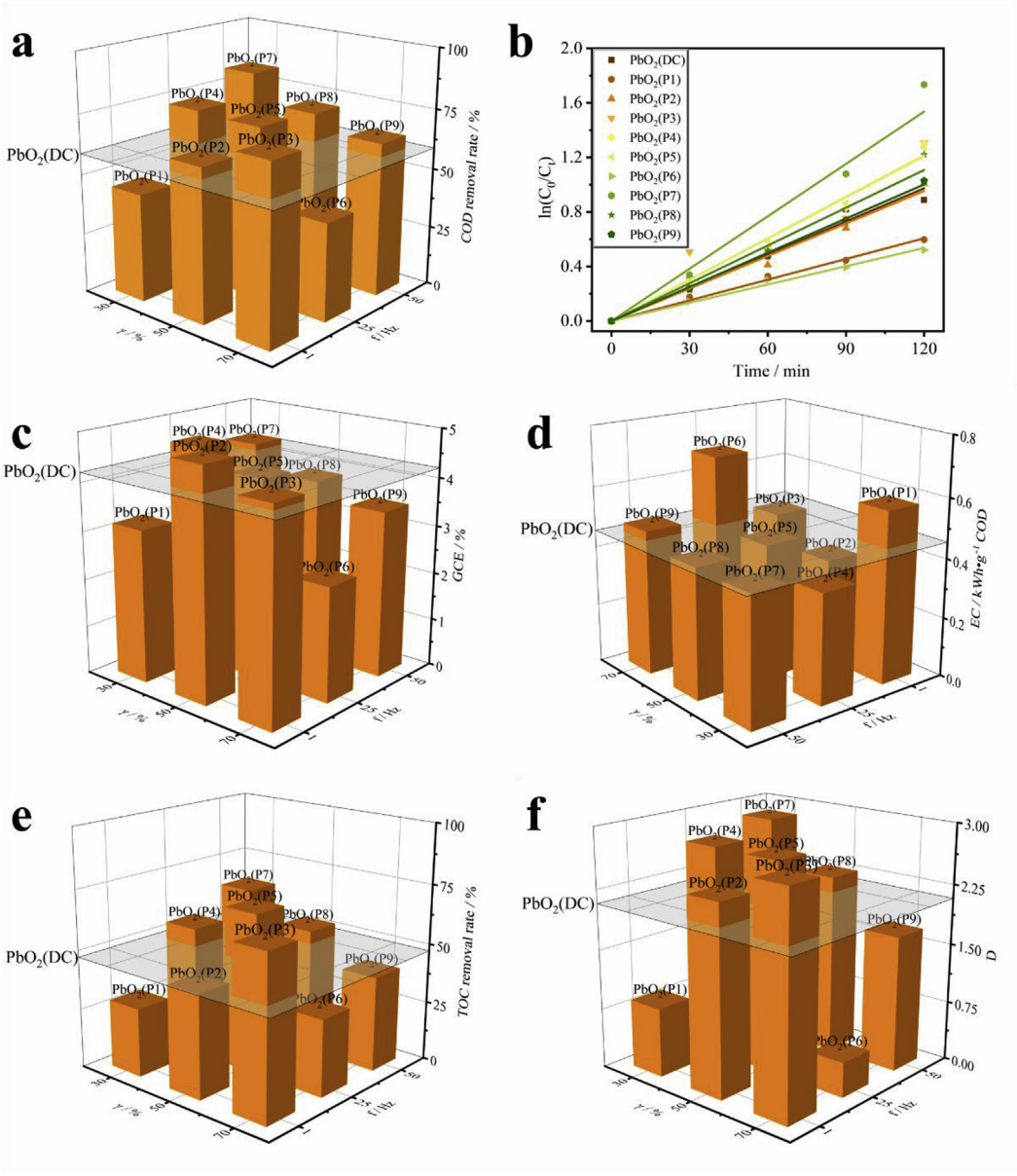

Fig. 6. AR1 degradation results of prepared electrodes.

3.5. Electrode stability

According to the accelerated lifetime test results shown in Fig. SM-5 and Table 1, pulse electrodeposited PbO_2 electrodes exhibited greater stability than that of PbO_2(DC). The accelerated lifetime of PbO_2(P4) reached up to 272 h, which was the longest and 1.79 times as long as that of PbO_2(DC) (152 h). Comparing with previous studies about porous PbO_2 electrode (Xu et al., 2019a), the accelerated lifetime of PbO_2(P4) was much longer. The lifetime increase of pulse electrodeposited PbO_2 could be explained by that pulse electrodeposition makes the PbO_2 surface more compact, preventing the penetration of electrolyte, thus conducive to improve the stability of PbO_2 electrode (He et al., 2019; Zhang et al., 2020).

The orthogonal analysis results are displayed in Table SM-9. The t and J_a were main influence factors on the accelerated lifetime of PbO_2 electrode. The accelerated lifetime positively correlates to those two parameters which are highly correlated with the average weight increase of PbO_2 layer (Table SM-10). It means that average weight increase of PbO_2 layer is crucial for extending service life of PbO_2 electrode.

Fig. SM-6 shows the Pb^{2+} leakage of prepared electrodes after 2 h electrolysis in 0.1 M Na_2SO_4 solution. All electrodes fabricated by pulse electrodeposition exhibited better safety than that of PbO_2(DC) except PbO_2(P3) and PbO_2(P4). It is because fine grain size and compact surface could promote the anti-corrosion ability of PbO_2 electrode. According to the average weight increase (Fig. SM-7), the high Pb^{2+} leakage of PbO_2(P3) and PbO_2(P4) could be ascribed to the high weight augment.

4. Conclusions

PbO_2 electrodes with different morphology and characters were successfully fabricated by pulse electrodeposition. SEM and XRD results indicated that pulse electrodeposition was conducive to fabricate uniform and compact structure. Electrochemical test

results suggested that pulse electrodeposition facilitated charge exchange. Hydroxide radical productivity test results revealed that pulse electrodeposition was helpful to create more active sites which highly correlates with hydroxide radical productivity. PbO_2(P7) exhibited the best electrochemical oxidation ability. The COD and R_{TOC} of PbO_2(P7) was 82.3% and 64.0% respectively. Accelerated lifetime and Pb^{2+} leakage test results showed that pulse electrodeposition could evidently promote the stability of PbO_2 electrode. Orthogonal analysis indicated that f positively correlated with voltammetry charge and hydroxide radical productivity. Whereas, J_a was the major influence factor on comprehensive electrochemical degradation performance of PbO_2 electrode. The influences of four factors can be ranked as follow: $J_a > \gamma \approx t > f$. In addition, the J_a and t presents highly positive correlation with electrode stability. Considering the degradation performance and electrode stability, the optimal parameters of pulse electrodeposition were: f = 50Hz, γ = 30%, J_a = 25 mA cm^{-2}, t = 60 min.

Together, based on aforesaid results, the pulse electrodeposition mechanism could be revealed and roughly concluded as follows: (i) Pulse current supply mode will not essentially change the basic PbO_2 electrodeposition mechanism. (ii) Pulse frequency(f) and duty ratio(γ) influence PbO_2 structure and morphology by adjusting the concentration polarization during electrodeposition process. (iii) Average current density(J_a) and deposition time(t) together decide total content of PbO_2 attached through electrodeposition. (iv) The combination of high f, low γ, large J_a and enough t could fabricate uniform and compact PbO_2 layer with fine crystal size, which shows great degradation performance and stability.

CRediT authorship contribution statement

Guo Hua: Conceptualization, Methodology, Investigation, Writing - original draft. **Xu Zhicheng:** Writing - review & editing. **Qiao Dan:** Methodology, Investigation. **Wan Dan:** Methodology, Investigation. **Xu Hao:** Conceptualization, Methodology, Writing - review & editing. **Yan Wei:** Supervision, Writing - review & editing. **Jin Xiaoliang:** Supervision, Writing - review & editing.

Declaration of competing interest

The authors declare that they have no known competing financial interests or personal relationships that could have appeared to influence the work reported in this paper.

Acknowledgement

The authors appreciatively acknowledge the financial support from the Key R&D Programs in Shaanxi Province (Program No. 2018SF-372) and Water Science and Technology Projects Foundation of SWAG (Program No. 2018SWAG0203).

Appendix A. Supplementary data

Supplementary data to this article can be found online at https://doi.org/10.1016/j.chemosphere.2020.128157.

References

Ansari, A., Nematollahi, D., 2020. Convergent paired electrocatalytic degradation of p-dinitrobenzene by Ti/SnO_2-Sb/beta-PbO_2 anode. A new insight into the electrochemical degradation mechanism. Appl. Catal. B Environ. 261, 12. https://doi.org/10.1016/j.apcatb.2019.118226.

Baddouh, A., El Ibrahimi, B., Rguitti, M.M., Mohamed, E., Hussain, S., Bazzi, L., 2019. Electrochemical removal of methylene bleu dye in aqueous solution using Ti/RuO_2-IrO_2 and SnO_2 electrodes. Separ. Purif. Technol. 55, 1852–1861. https://doi.org/10.1080/01496395.2019.1608244.

Bi, Q., Guan, W.Z., Gao, Y., Cui, Y.R., Ma, S.W., Xue, J.Q., 2019. Study of the mechanisms underlying the effects of composite intermediate layers on the performance of Ti/SnO_2-Sb-La electrodes. Electrochim. Acta 306, 667–679. https://doi.org/10.1016/j.electacta.2019.03.122.

Bian, X.Z., Xia, Y., Zhan, T.T., Wang, L., Zhou, W., Dai, Q.Z., Chen, J.M., 2019. Electrochemical removal of amoxicillin using a Cu doped PbO_2 electrode: electrode characterization, operational parameters optimization and degradation mechanism. Chemosphere 233, 762–770. https://doi.org/10.1016/j.chemosphere.2019.05.226.

Boukhchina, S., Akrout, H., Berling, D., Bousselmi, L., 2019. Highly efficient modified lead oxide electrode using a spin coating/electrodeposition mode on titanium for electrochemical treatment of pharmaceutical pollutant. Chemosphere 221, 356–365. https://doi.org/10.1016/j.chemosphere.2019.01.057.

Chaplin, B.P., 2014. Critical review of electrochemical advanced oxidation processes for water treatment applications. Environ. Sci.-Process Impacts 16, 1182–1203. https://doi.org/10.1039/c3em00679d.

Chen, M., Wang, C., Wang, Y.C., Meng, X.Y., Chen, Z.F., Zhang, W.Q., Tan, G., 2019. Kinetic, mechanism and mass transfer impact on electrochemical oxidation of MIT using Ti-enhanced nanotube arrays/SnO_2-Sb anode. Electrochim. Acta 323, 11. https://doi.org/10.1016/j.electacta.2019.134779.

Chen, S., Li, J., Liu, L., He, Q., Zhou, L., Yang, T., Wang, X., He, P., Zhang, H., Jia, B., 2020. Fabrication of Co/Pr co-doped Ti/PbO_2 anode for efficiently electrocatalytic degradation of beta-naphthoxyacetic acid. Chemosphere 256, 127139. https://doi.org/10.1016/j.chemosphere.2020.127139.

Cornejo, O.M., Murrieta, M.F., Castaneda, L.F., Nava, J.L., 2020. Characterization of the reaction environment in flow reactors fitted with BDD electrodes for use in electrochemical advanced oxidation processes: a critical review. Electrochim. Acta 331. https://doi.org/10.1016/j.electacta.2019.135373.

Dargahi, A., Ansari, A., Nematollahi, D., Asgari, G., Shokoohi, R., Samarghandi, M.R., 2019. Parameter optimization and degradation mechanism for electrocatalytic degradation of 2,4-diclorophenoxyacetic acid (2,4-D) herbicide by lead dioxide electrodes. RSC Adv. 9, 5064–5075. https://doi.org/10.1039/c8ra10105a.

Duan, X.Y., Sui, X.Y., Wang, W.Y., Bai, W.H., Chang, L.M., 2019. Fabrication of PbO_2/SnO_2 composite anode for electrochemical degradation of 3-chlorophenol in aqueous solution. Appl. Surf. Sci. 494, 211–222. https://doi.org/10.1016/j.apsusc.2019.07.161.

Duan, X.Y., Xu, F., Wang, Y.N., Chen, Y.W., Chang, L.M., 2018. Fabrication of a hydrophobic SDBS-PbO_2 anode for electrochemical degradation of nitrobenzene in aqueous solution. Electrochim. Acta 282, 662–671. https://doi.org/10.1016/j.electacta.2018.06.098.

Elaissaoui, I., Akrout, H., Grassini, S., Fulginiti, D., Bousselmi, L., 2019. Effect of coating method on the structure and properties of a novel PbO_2 anode for electrochemical oxidation of Amaranth dye. Chemosphere 217, 26–34. https://doi.org/10.1016/j.chemosphere.2018.10.161.

Hakimi, F., Rashchi, F., Dolati, A., Astaraei, F.R., 2019. Anodizing Pb electrode for synthesis of beta-PbO_2 nanoparticles: optimization of electrochemical parameters. J. Electrochem. Soc. 166, D617–D625. https://doi.org/10.1149/2.0551913jes.

He, X.H., Xu, P.F., Mao, J.W., Tang, Y.M., 2019. Electrodeposition and performance of Ti/SnO_2-Sb/PbO_2 electrodes from methanesulfonate baths. J. Electrochem. Soc. 166, D452–D459. https://doi.org/10.1149/2.1321910jes.

He, Z., Hayat, M.D., Huang, S.F., Wang, X.G., Cao, P., 2018. PbO_2 electrodes prepared by pulse reverse electrodeposition and their application in benzoic acid degradation. J. Electroanal. Chem. 812, 74–81. https://doi.org/10.1016/j.jelechem.2018.01.044.

Hu, Z.X., Zhou, M.H., Zhou, L., Li, Y.L., Zhang, C., 2014. Effect of matrix on the electrochemical characteristics of TiO_2 nanotube array-based PbO_2 electrode for pollutant degradation. Environ. Sci. Pollut. Res. 21, 8476–8484. https://doi.org/10.1007/s11356-014-2792-0.

Lei, Jiani, Xu, Zhicheng, Yuan, Xiaoqi, Xu, Hao*, Qiao, Dan, Liao, Zhengwei, Yan, Wei, Yu, W., 2020. Linear attenuation current input mode: a novel power supply mode for electrochemical oxidation process. J. Water Process Eng. 36, 101305 https://doi.org/10.1016/j.jwpe.2020.101305.

Lei Jiani, X.Z., Xu, Hao, Qiao, Dan, Liao, Zhengwei, Yan, Wei, Wang, Yu, 2020. Pulsed electrochemical oxidation of acid red G and crystal violet by PbO_2 anode. J. Environ. Chem. Eng. 8, 103773 https://doi.org/10.1016/j.jece.2020.103773.

Li, X., Xu, H., Yan, W., 2016a. Fabrication and characterization of a PbO_2-TiN composite electrode by co-deposition method. J. Electrochem. Soc. 163, D592–D602. https://doi.org/10.1149/2.0261610jes.

Li, X., Xu, H., Yan, W., 2017. Effects of twelve sodium dodecyl sulfate (SDS) on electro-catalytic performance and stability of PbO_2 electrode. J. Alloys Compd. 718, 386–395. https://doi.org/10.1016/j.jallcom.2017.05.147.

Li, X.L., Xu, H., Yan, W., 2016b. Fabrication and characterization of PbO_2 electrode modified with polyvinylidene fluoride (PVDF). Appl. Surf. Sci. 389, 278–286. https://doi.org/10.1016/j.apsusc.2016.07.123.

Lin, H., Niu, J.F., Liang, S.T., Wang, C., Wang, Y.J., Jin, F.Y., Luo, Q., Huang, Q.G., 2018. Development of macroporous Magneli phase Ti_4O_7 ceramic materials: as an efficient anode for mineralization of poly- and perfluoroalkyl substances. Chem. Eng. J. 354, 1058–1067. https://doi.org/10.1016/j.cej.2018.07.210.

Liu, S.Q., Wang, Y., Zhou, X.Z., Han, W.Q., Li, J.S., Sun, X.Y., Shen, J.Y., Wang, L.J., 2017. Improved degradation of the aqueous flutriafol using a nanostructure macroporous PbO_2 as reactive electrochemical membrane. Electrochim. Acta 253, 357–367. https://doi.org/10.1016/j.electacta.2017.09.055.

Lyu, J.H., Han, H.B., Wu, Q., Ma, H.C., Ma, C., Dong, X.L., Fu, Y.H., 2019. Enhancement

of the electrocatalytic oxidation of dyeing wastewater (reactive brilliant blue KN-R) over the Ce-modified Ti-PbO_2 electrode with surface hydrophobicity. J. Solid State Electrochem. 23, 847–859. https://doi.org/10.1007/s10008-018-04170-9.

Mei, R., Wei, Q., Zhu, C., Ye, W., Zhou, B., Ma, L., Yu, Z., Zhou, K., 2019. 3D macroporous boron-doped diamond electrode with interconnected liquid flow channels: a high-efficiency electrochemical degradation of RB-19 dye wastewater under low current. Appl. Catal. B Environ. 245, 420–427. https://doi.org/10.1016/j.apcatb.2018.12.074.

Miklos, D.B., Remy, C., Jekel, M., Linden, K.G., Drewes, J.E., Huebner, U., 2018. Evaluation of advanced oxidation processes for water and wastewater treatment - a critical review. Water Res. 139, 118–131. https://doi.org/10.1016/j.watres.2018.03.042.

Nidheesh, P.V., Zhou, M., Oturan, M.A., 2018. An overview on the removal of synthetic dyes from water by electrochemical advanced oxidation processes. Chemosphere 197, 210–227. https://doi.org/10.1016/j.chemosphere.2017.12.195.

Panizza, M., Cerisola, G., 2009. Direct and mediated anodic oxidation of organic pollutants. Chem. Rev. 109, 6541–6569. https://doi.org/10.1021/cr9001319.

Qian, S., Liu, S., Jiang, Z.Y., Deng, D.L., Tang, B.B., Zhang, J.Z., 2019. Electrochemical degradation of tetracycline antibiotics using a Ti/SnO_2-Sb_2O_3/PbO_2 anode: kinetics, pathways, and biotoxicity change. J. Electrochem. Soc. 166, E192–E199. https://doi.org/10.1149/2.1411906jes.

Rao, A.N.S., Venkatarangaiah, V.T., 2014. Metal oxide-coated anodes in wastewater treatment. Environ. Sci. Pollut. Res. 21, 3197–3217. https://doi.org/10.1007/s11356-013-2313-6.

Shao, D., Lyu, W., Cui, J., Zhang, X., Zhang, Y., Tan, G., Yan, W., 2020. Polyaniline nanoparticles magnetically coated Ti/Sb-SnO_2 electrode as a flexible and efficient electrocatalyst for boosted electrooxidation of biorefractory wastewater. Chemosphere 241, 125103. https://doi.org/10.1016/j.chemosphere.2019.125103.

Sirés, I., Low, C.T.J., Ponce-de-León, C., Walsh, F.C., 2010. The characterisation of PbO_2-coated electrodes prepared from aqueous methanesulfonic acid under controlled deposition conditions. Electrochim. Acta 55, 2163–2172. https://doi.org/10.1016/j.electacta.2009.11.051.

Sun, D., Hong, X., Wu, K., Hui, K.S., Du, Y., Hui, K.N., 2020. Simultaneous removal of ammonia and phosphate by electro-oxidation and electrocoagulation using RuO_2-IrO_2/Ti and microscale zero-valent iron composite electrode. Water Res. 169, 115239. https://doi.org/10.1016/j.watres.2019.115239.

Sun, T., Wang, J.R., Liu, Y.J., Wang, J., Wang, L.F., Jiang, B., 2019. A comprehensive study on nano-diamond doped beta-PbO_2 electrode: preparation, properties and electrocatalytic performance. J. Electrochem. Soc. 166, E473–E480. https://doi.org/10.1149/2.0591914jes.

Suzuki, N., Okazaki, A., Kuriyama, H., Serizawa, I., Hirami, Y., Hara, A., Hirano, Y., Nakabayashi, Y., Roy, N., Terashima, C., Nakata, K., Katsumata, K.-i., Kondo, T., Yuasa, M., Fujishima, A., 2020. Synergetic effect in water treatment with mesoporous TiO_2/BDD hybrid electrode. RSC Adv. 10, 1793–1798. https://doi.org/10.1039/c9ra10318j.

Tammam, R.H., Hassan, H.B., 2019. Enhancement of urea electrooxidation on PbO_2-Ni/C and Bi_2O_3-Ni/C nanocomposites in Alkaline medium. J. Electrochem. Soc. 166, F729–F745. https://doi.org/10.1149/2.0371912jes.

Tang, C.-b., Lu, Y.-x., Wang, F., Niu, H., Yu, L.-h., Xue, J.-q., 2020. Influence of a MnO_2-WC interlayer on the stability and electrocatalytic activity of titanium-based PbO_2 anodes. Electrochim. Acta 331, 135381. https://doi.org/10.1016/j.electacta.2019.135381.

Velichenko, A., Luk'yanenko, T., Shmychkova, O., Dmitrikova, L., 2020. Electrosynthesis and catalytic activity of PbO_2-fluorinated surfactant composites. J. Chem. Technol. Biotechnol., 6483 https://doi.org/10.1002/jctb.6483. In press.

Velichenko, A.B., Amadelli, R., Gruzdeva, E.V., Luk'yanenko, T.V., Danilov, F.I., 2009. Electrodeposition of lead dioxide from methanesulfonate solutions. J. Power Sources 191, 103–110. https://doi.org/10.1016/j.jpowsour.2008.10.054.

Wang, C., Niu, J.F., Yin, L.F., Huang, J.X., Hou, L.A., 2018. Electrochemical degradation of fluoxetine on nanotube array intercalated anode with enhanced electronic transport and hydroxyl radical production. Chem. Eng. J. 346, 662–671. https://doi.org/10.1016/j.cej.2018.03.159.

Wang, G., Liu, Y., Ye, J., Lin, Z., Yang, X., 2020. Electrochemical oxidation of methyl orange by a Magneli phase Ti_4O_7 anode. Chemosphere 241, 125084. https://doi.org/10.1016/j.chemosphere.2019.125084.

Wang, Y.C., Chen, M., Wang, C., Meng, X.Y., Zhang, W.Q., Chen, Z.F., Crittenden, J., 2019. Electrochemical degradation of methylisothiazolinone by using Ti/SnO_2-Sb_2O_3/alpha, beta-PbO_2 electrode: kinetics, energy efficiency, oxidation mechanism and degradation pathway. Chem. Eng. J. 374, 626–636. https://doi.org/10.1016/j.cej.2019.05.217.

Wang, Z.C., Mao, Y.L., Xu, M., Wei, Y.J., Hu, Y.H., Zhu, C.G., Fang, W.Y., Wang, F.W., 2017. Fabrication and enhanced electrocatalytic activity of three-dimensional sphere-stacking PbO_2 coatings based on TiO_2 nanotube arrays substrate for the electrochemical oxidation of organic pollutants. J. Electrochem. Soc. 164, H981–H988. https://doi.org/10.1149/2.0151714jes.

Weng, M.L., Yu, X.H., 2019. Electrochemical oxidation of para-aminophenol with rare earth doped lead dioxide electrodes: kinetics modeling and mechanism. Front. Chem. 7, 00382 https://doi.org/10.3389/fchem.2019.00382.

Wu, J., Zhu, K., Xu, H., Yan, W., 2019. Electrochemical oxidation of rhodamine B by PbO_2/Sb-SnO_2/TiO_2 nanotube arrays electrode. Chin. J. Catal. 40, 917–927. https://doi.org/10.1016/s1872-2067(19)63342-5.

Xia, Y.J., Dai, Q.Z., 2018. Electrochemical degradation of antibiotic levofloxacin by PbO_2 electrode: kinetics, energy demands and reaction pathways. Chemosphere 205, 215–222. https://doi.org/10.1016/j.chemosphere.2018.04.103.

Xu, F., Chang, L.M., Duan, X.Y., Bai, W.H., Sui, X.Y., Zhao, X.S., 2019a. A novel layer-by-layer CNT/PbO_2 anode for high-efficiency removal of PCP-Na through combining adsorption/electrosorption and electrocatalysis. Electrochim. Acta 300, 53–66. https://doi.org/10.1016/j.electacta.2019.01.090.

Xu, H., Guo, W.Q., Wu, J., Feng, J.T., Yang, H.H., Yan, W., 2016. Preparation and characterization of titanium-based PbO_2 electrodes modified by ethylene glycol. RSC Adv. 6, 7610–7617. https://doi.org/10.1039/c5ra21195f.

Xu, K.D., Peng, J.H., Chen, P., Gu, W.K., Luo, Y.B., Yu, P., 2019b. Preparation and characterization of porous Ti/SnO_2-Sb_2O_3/PbO_2 electrodes for the removal of chloride ions in water. Processes 7, 14. https://doi.org/10.3390/pr7100762.

Xu, M., Mao, Y.L., Song, W.L., OuYang, X.M., Hu, Y.H., Wei, Y.J., Zhu, C.G., Fang, W.Y., Shao, B.C., Lu, R., Wang, F.W., 2018. Preparation and characterization of Fe-Ce co-doped Ti/TiO_2 NTs/PbO_2 nanocomposite electrodes for efficient electrocatalytic degradation of organic pollutants. J. Electroanal. Chem. 823, 193–202. https://doi.org/10.1016/j.jelechem.2018.06.007.

Xu, P.F., He, X.H., Mao, J.W., Tang, Y.M., 2019c. Fabrication of Ti/SnO_2-Sb/Ce-PbO_2 anode from methanesulfonate bath and its electrocatalytic activity. J. Electrochem. Soc. 166, D638–D644. https://doi.org/10.1149/2.1031913jes.

Yang, W., Yang, W., Lin, X., 2012. Research on PEG modified Bi-doping lead dioxide electrode and mechanism. Appl. Surf. Sci. 258, 5722. https://doi.org/10.1016/j.apsusc.2012.02.073.

Yang, Y., Cui, L.L., Li, M.Y., Yao, Y.W., 2019. Electrochemical removal of metribuzin in aqueous solution by a novel PbO_2/WO_3 composite anode: characterization, influencing parameters and degradation pathways. J. Taiwan Inst. Chem. Eng. 102, 170–181. https://doi.org/10.1016/j.jtice.2019.05.023.

Yao, Y.W., Dong, H.S., Yu, N.C., Chen, X., Jiao, L.M., Zhao, C.M., 2017. Effects of peak current density on the structure and property of PbO_2-CeO_2 nanocomposite electrodes prepared by pulse electrodeposition. Russ. J. Electrochem. 53, 411–416. https://doi.org/10.1134/s1023193517020148.

Yao, Y.W., Li, M.Y., Yang, Y., Cui, L.L., Guo, L., 2019a. Electrochemical degradation of insecticide hexazinone with Bi-doped PbO_2 electrode: influencing factors, intermediates and degradation mechanism. Chemosphere 216, 812–822. https://doi.org/10.1016/j.chemosphere.2018.10.191.

Yao, Y.W., Ren, B.L., Yang, Y., Huang, C.J., Li, M.Y., 2019b. Preparation and electrochemical treatment application of Ce-PbO_2/ZrO_2 composite electrode in the degradation of acridine orange by electrochemical advanced oxidation process. J. Hazard Mater. 361, 141–151. https://doi.org/10.1016/j.jhazmat.2018.08.081.

Ye, F., Wang, Z., Xu, C., Yuan, M., Liu, P., Yang, W., Liu, G., 2020. Mechanism and kinetic study of pulse electrodeposition process of Pt/C catalysts for fuel cells. Renew. Energy 145, 514–520. https://doi.org/10.1016/j.renene.2019.06.034.

Ye, F., Xu, C., Liu, G., Yuan, M., Wang, Z., Du, X., Lee, J.K., 2018. Effect of pulse electrodeposition parameters on electrocatalytic the activity of methanol oxidation and morphology of Pt/C catalyst for direct methanol fuel cells. Energy Convers. Manag. 160, 85–92. https://doi.org/10.1016/j.enconman.2018.01.027.

Yijing Xia, X.B., Xia, Yi, Zhou, Wan, Wang, Lin, Fan, Siqi, Pan, Xiong, Zhan, Tingting, Dai, Qizhou, Chen, Jianmeng, 2020. Effect of indium doping on the PbO_2 electrode for the enhanced electrochemical oxidation of aspirin: an electrode comparative study. Separ. Purif. Technol. 237, 116321. https://doi.org/10.1016/j.seppur.2019.116321.

Yu, H.B., Song, Y.N., Zhao, B., Lu, Y., Zhu, S.Y., Qu, J., Wang, X.H., Qin, W.C., 2018. Efficient electrocatalytic degradation of 4-chlorophenol using a Ti/RuO_2-SnO_2-TiO_2/PbO_2-CeO_2 composite electrode. Electrocatalysis 9, 725–734. https://doi.org/10.1007/s12678-018-0484-0.

Yuan, M., Salman, N.M., Guo, H., Xu, Z., Xu, H., Yan, W., Liao, Z., Wang, Y., 2019. A 2.5D electrode system constructed of magnetic Sb–SnO_2 particles and a PbO_2 electrode and its electrocatalysis application on acid red G degradation. Catalysts 9, 875. https://doi.org/10.3390/catal9110875.

Zahorulko, S., Shmychkova, O., Luk'yanenko, T., Dmitrikova, L., Velichenko, A., 2019. The comparative study of electrocatalytic activity of various anode materials in respect to the oxidation of nitroanilines. Mater. Today-Proc. 6, 242–249. https://doi.org/10.1016/j.matpr.2018.10.101.

Zhang, M., Shi, Q., Song, X.Z., Wang, H., Bian, Z.Y., 2019a. Recent electrochemical methods in electrochemical degradation of halogenated organics: a review. Environ. Sci. Pollut. Res. 26, 10457–10486. https://doi.org/10.1007/s11356-019-04533-3.

Zhang, W., Li, H., Ma, Z., Li, H., Wang, H., 2019b. Photocatalytic degradation of azophloxine on porous $La_2Ti_2O_7$ prepared by sol-gel method. Solid State Sci. 87, 58–63. https://doi.org/10.1016/j.solidstatesciences.2018.11.004.

Zhang, X., Shao, D., Lyu, W., Tan, G., Ren, H., 2019c. Utilizing discarded SiC heating rod to fabricate SiC/Sb-SnO_2 anode for electrochemical oxidation of wastewater. Chem. Eng. J. 361, 862–873. https://doi.org/10.1016/j.cej.2018.12.085.

Zhang, Y., He, P., Zhou, L., Dong, F., Yang, D., Lei, H., Dua, L., Jia, L., Zhou, S., 2020. Optimized terbium doped Ti/PbO_2 dimensional stable anode as a strong tool for electrocatalytic degradation of imidacloprid waste water. Ecotoxicol. Environ. Saf. 188, 109921 https://doi.org/10.1016/j.ecoenv.2019.109921.

Zhou, Y., Li, Z., Hao, C., Zhang, Y., Chai, S., Han, G., Xu, H., Lu, J., Dang, Y., Sun, X., Fu, Y., 2020. Electrocatalysis enhancement of alpha, beta-PbO_2 nanocrystals induced via rare earth Er(III) doping strategy: principle, degradation application and electrocatalytic mechanism. Electrochim. Acta 333, 135535. https://doi.org/10.1016/j.electacta.2019.135535.